Smart Mater. Struct. **18** (2009) 104014 (6pp) doi:10.1088/0964-1726/18/10/104014

# Dynamic sensing behavior of ferromagnetic shape memory Ni–Mn–Ga*

**N N Sarawate**[1] **and M J Dapino**[2]

[1] GE Global Research Center, Niskayuna NY, 12309, USA
[2] Department of Mechanical Engineering, Ohio State University, Columbus, OH 43210, USA

E-mail: sarawate@ge.com and dapino.1@osu.edu

Received 29 January 2009, in final form 3 August 2009
Published 10 September 2009
Online at stacks.iop.org/SMS/18/104014

**Abstract**
This paper is focused on the characterization and modeling of a commercial Ni–Mn–Ga alloy for use as a dynamic deformation sensor. The flux density is experimentally determined as a function of cyclic strain loading at frequencies from 0.2 to 160 Hz. With increasing frequency, the stress versus strain response remains almost unchanged whereas the flux density versus strain response shows increasing hysteresis. This behavior indicates that twin-variant reorientation occurs in concert with the mechanical loading, whereas the rotation of magnetization vectors occurs with a delay as the loading frequency increases. The increasing hysteresis in magnetization must be considered when utilizing the material in dynamic sensing applications. A modeling strategy is developed which incorporates magnetic diffusion and a linear constitutive equation. The model is used to describe the hysteretic dependence of magnetic flux density on strain at dynamic frequencies.

(Some figures in this article are in colour only in the electronic version)

## 1. Introduction

A major advantage of ferromagnetic shape memory alloys (FSMAs) in the Ni–Mn–Ga system over the thermally activated shape memory alloys (SMAs) is their ability to produce large strains of around 6% at a high-frequency bandwidth in the kilohertz range. Extensive work exists on the quasi-static behavior of these materials (see the review papers [1, 2]). However, the characterization and modeling of Ni–Mn–Ga under dynamic mechanical or magnetic excitation has received only limited attention.

Henry [3] presented measurements of magnetic-field-induced strains of up to 3% for drive field frequencies up to 250 Hz and a linear model to describe the phase lag between strain and field and system resonance frequencies. Peterson [4] presented dynamic actuation measurements on piezoelectrically assisted twin boundary motion in Ni–Mn–Ga. The acoustic stress waves produced by a piezoelectric actuator complement the externally applied fields and allow for reduced field strengths. Marioni *et al* [5] presented pulsed magnetic field actuation of Ni–Mn–Ga for field pulses lasting up to 620 $\mu$s. The complete field-induced strain was observed to occur in 250 $\mu$s, indicating the possibility of obtaining cyclic 6% strain for frequencies up to 2000 Hz. Weetman and Akhras [6] presented a model that employs a modified Euler–Lagrange equation to simulate dynamic strain versus field behavior. Gauthier *et al* [7, 8] presented the design and modeling of a control scheme for a mechatronic system using FSMAs. Magnetization measurements and models were not reported in these studies as they are usually not critical for actuation applications. Faidley *et al* [9] and Sarawate and Dapino [10] presented frequency response measurements of acceleration transmissibility using mechanical base excitation to investigate the effect of bias fields on the stiffness of Ni–Mn–Ga. However, the magnitude of base acceleration was not sufficient to induce twin boundary motion and associated magnetization changes.

The sensing effect in Ni–Mn–Ga refers to the action of external mechanical stress on the magnetic properties of the material. Only a few studies exist on the sensing effect of Ni–Mn–Ga [11–17] as compared to the actuation effect. Mullner *et al* [11] experimentally studied strain-induced changes in the flux density under external quasi-static loading at a constant field of 558 kA m$^{-1}$. Straka and Heczko [12] reported superelastic response for fields higher than 239 kA m$^{-1}$ and established the interconnection between

* This work was performed by the authors at The Ohio State University.

 

magnetization and strain. Heczko [16] further investigated this interconnection and proposed a simple energy model. Suorsa *et al* [13] reported magnetization measurements for various discrete strain and field intensities ranging between 0% and 6% and 5 and 120 kA m$^{-1}$, respectively. Sarawate and Dapino [17] reported flux density change due to 6% strain input at bias fields ranging from 0 to 445 kA m$^{-1}$, and presented a continuum thermodynamics model [18] for the sensing effect. However, all of these studies are concerned with quasi-static magnetization response and an investigation on the effect of dynamic mechanical input on the magnetization of Ni–Mn–Ga has been lacking. Recently, Karaman *et al* [19] reported voltage measurements in a pickup coil due to flux density change under a dynamic strain loading of 4.9% at frequencies in the 0.5–10 Hz range, from the viewpoint of energy harvesting. Their study presents the highest frequency of mechanical loading to date which induces twin boundary motion in Ni–Mn–Ga (10 Hz). However, the dependence of flux density on strain was not reported.

Prior investigations including our previous work [10, 17, 18, 20] have not dealt with modeling and characterization of Ni–Mn–Ga subjected to dynamic mechanical loading. In this paper we characterize the dependence of flux density and stress on dynamic strain at a bias field of 368 kA m$^{-1}$ for frequencies up to 160 Hz, with a view to determining the feasibility of using Ni–Mn–Ga as a dynamic deformation sensor. This value of bias field was determined to be optimum for obtaining maximum reversible flux density change [17]. The measurements also illustrate the dynamic behavior of twin boundary motion and magnetization rotation in Ni–Mn–Ga. A modeling strategy is developed using a linear constitutive equation and magnetic diffusion.

## 2. Experimental characterization

Figure 1 shows the experimental set-up, which consists of a custom-designed electromagnet and a uniaxial MTS 831 test frame. This frame is designed for cyclic fatigue loading, with special servo valves which allow precise stroke control for frequencies up to 200 Hz. The set-up is similar to that described in [17] for characterization of the quasi-static sensing behavior. A 6 × 6 × 10 mm$^3$ single-crystal Ni–Mn–Ga sample (AdaptaMat Ltd.) is placed in the center gap of the electromagnet. In the low-temperature martensite phase, the sample exhibits a free magnetic-field-induced deformation of 5.8% under a transverse field of 700 kA m$^{-1}$. The material is first converted to a single field-preferred variant by applying a high field along the transverse ($x$) direction. The field is removed and the material is then slowly compressed by 3.1% at a bias field of 368 kA m$^{-1}$ applied in the $x$ direction. While being exposed to the bias field, the sample is subjected to a cyclic uniaxial strain loading of 3% amplitude (peak to peak) along the longitudinal ($y$) direction at a desired frequency. This process is repeated for frequencies ranging between 0.2 and 160 Hz. The flux density inside the material is measured by a Hall probe placed in the gap between a magnet pole and a face of the sample. The Hall probe measures the net flux density along the $x$ direction, from which the $x$-axis magnetization

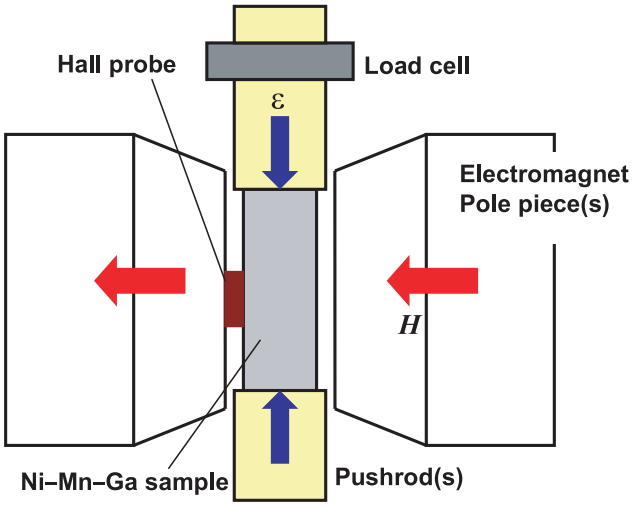


**Figure 1.** Experimental set-up for dynamic magnetization measurements.

can be calculated. The compressive force is measured by a load cell and the displacement is measured by a linear variable differential transducer. The data is recorded using data acquisition software at a sampling frequency of 4096 Hz. All the measuring instruments have a bandwidth in the kilohertz range, well above the highest frequency employed in the study.

Figure 2(a) shows stress versus strain measurements for frequencies ranging from 4 to 160 Hz. The strain axis is biased around the initial strain of 3.1%. These plots show typical pseudoelastic minor loop behavior associated with single-crystal Ni–Mn–Ga at a high bias field. With increasing compressive strain, the stress increases elastically until a critical value is reached, beyond which twin boundary motion starts and the stress-preferred variants grow at the expense of the field-preferred variants. During unloading, the material exhibits pseudoelastic reversible behavior because the bias field of 368 kA m$^{-1}$ results in the generation of field-preferred variants at the expense of stress-preferred variants.

The flux density dependence on strain shown in figure 2(b) is of interest for sensing applications. The absolute value of flux density decreases with increasing compression. Due to the high magnetocrystalline anisotropy of Ni–Mn–Ga, the nucleation and growth of stress-preferred variants during compression are accompanied by rotation of magnetization vectors into the longitudinal direction, which causes a reduction of the permeability and flux density in the transverse direction. The magnetically easy crystallographic axis is termed the $c$ axis, whereas the hard axis is termed the $a$ axis. At low frequencies up to 4 Hz, the flux density dependence on strain is almost linear with little hysteresis. The data at 0.2 Hz is not shown in the figures as it matches the data at 4 Hz. This low-frequency behavior is consistent with some of the previous observations [16, 17, 21]. The net flux density change for a strain range of 3% is around 0.056 T (560 G) for almost all frequencies, which shows that the magnetization vectors rotate in the longitudinal direction by the same amount for all the frequencies investigated. The applied strain amplitude does not remain exactly at ±1.5% because the MTS controller

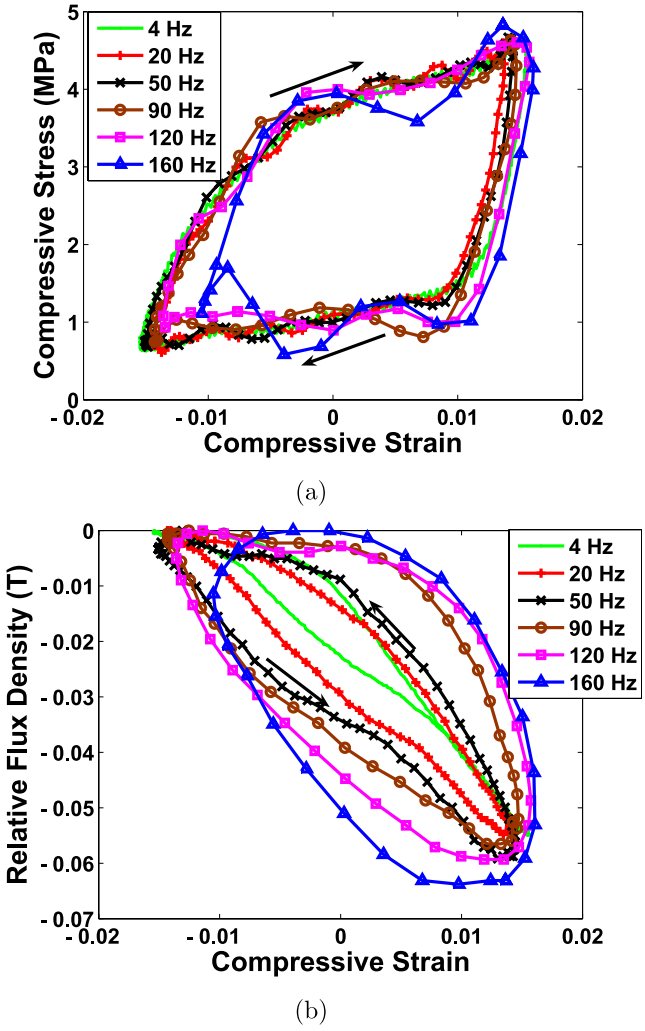


**Figure 2.** (a) Stress versus strain and (b) flux density versus strain measurements for frequencies up to 160 Hz.

is working at very low displacements (≈±0.15 mm) and high frequencies. Nevertheless, the strain amplitudes are maintained within a sufficiently narrow range (±8%) so that a comparative study is possible on a consistent basis for different frequencies.

With increasing frequency, the stress versus strain behavior remains relatively unchanged (figure 2(a)). The data at 160 Hz is slightly different to the other measurements as, at this frequency, the machine is operated close to its 200 Hz limit. Notwithstanding, the same overall behavior is observed. This indicates that twin-variant reorientation occurs in concert with the applied loading for the frequency range under consideration. This behavior is consistent with work by Marioni [5] showing that twin boundary motion occurs in concert with the applied field for frequencies up to 2000 Hz. On the other hand, the dependence of flux density ($B$) on strain ($\varepsilon$) shows a monotonic increase in hysteresis with increasing frequency. The hysteresis loss in the stress ($\sigma$) versus strain plots is equal to the area enclosed by one cycle ($\oint \sigma \,\mathrm{d}\varepsilon$), whereas the loss in the flux density versus strain plots is proportional to the enclosed area ($\oint B \,\mathrm{d}\varepsilon$) [22, 23]. The hysteresis loss proportional to the area enclosed by flux density versus strain plots is the magnetomechanical loss, $W_{\mathrm{me}}$.

For piezoelectric and magnetostrictive materials, which exhibit both elastic and field-induced deformations, their constitutive behavior is often described with linear functions which are approximately accurate when the material is biased and driven with small fields. Although Ni–Mn–Ga exhibits responses that are hysteretic even at low fields, at a given bias field the material response may be approximately described in an analogous fashion to piezoelectric materials [22] by

$$\sigma = f(\varepsilon) + qH, \tag{1}$$

$$M = e\varepsilon + \chi H, \tag{2}$$

where $H$ is the applied magnetic field, $M$ is the magnetization, $f(\varepsilon)$ is a hysteretic function of strain that is described through the nonlinear constitutive stress versus strain model presented in [18], $q$ is a coupling coefficient relating stress to bias magnetic field, $e$ is a coupling coefficient relating magnetization to strain and $\chi$ is magnetic susceptibility. For comparison with experimental data, the measured value of flux density ($B_{\mathrm{m}}$) is used:

$$B_{\mathrm{m}} = \mu_0(H + N_{\mathrm{d}}M), \tag{3}$$

where $N_{\mathrm{d}}$ is the demagnetization factor [18]. Equation (3) has a positive sign for term $N_{\mathrm{d}}M$ because $B_{\mathrm{m}}$ is the measured flux density on the outer surface of the sample. Equation (3) was shown to accurately quantify the magnetization inside the material from the measured flux density through a comparison with finite element analysis of the magnetic circuit (refer to appendix 2 of Sarawate [24]). Combination of (2) and (3) gives

$$B_{\mathrm{m}} = \mu_0 N_{\mathrm{d}} e\varepsilon + \mu_0(1 + N_{\mathrm{d}}\chi)H. \tag{4}$$

To quantify the magnetomechanical energy loss due to hysteresis, we follow a similar approach as done in [22]. The general expression for mechanical loss in one cycle is considered first,

$$W_{\mathrm{me}} = \oint \sigma \,\mathrm{d}\varepsilon. \tag{5}$$

From (1), the stress varies with magnetic field by relation $\sigma = qH$ at a given strain. Assuming $\varepsilon = 0$, equation (5) takes the form

$$W_{\mathrm{me}} = \oint qH \,\mathrm{d}\varepsilon. \tag{6}$$

Substitution into (6) of the magnetic field solution from (4) gives

$$W_{\mathrm{me}} = \frac{q}{\mu_0(1 + N_{\mathrm{d}}\chi)} \oint B_{\mathrm{m}} \,\mathrm{d}\varepsilon. \tag{7}$$

Equation (7) gives the magnetomechanical energy loss, which is proportional to the area enclosed by one cycle of a flux density versus strain plot. The coupling coefficient $q$ is approximated from the twinning stress versus magnetic field curve [18]. It is proposed that the effect of bias field is to shift the stress versus strain curve upwards by a constant amount. At 368 kA m$^{-1}$, the twinning stress versus field curve gives a coupling coefficient of $q = \sigma/H = 6.9735$ kg A$^{-1}$ s$^{-2}$.

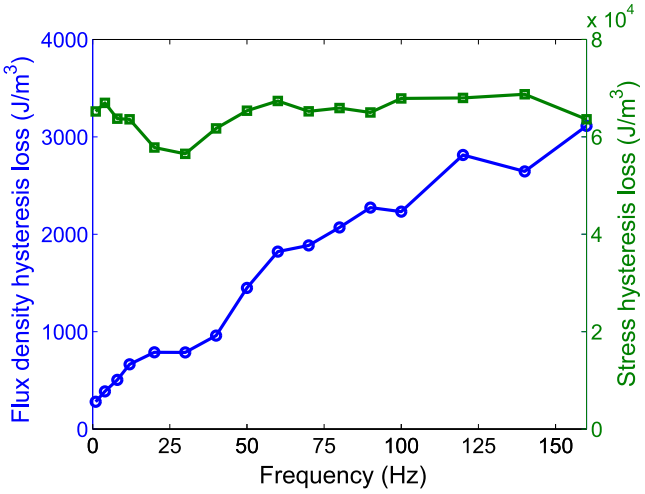


**Figure 3.** Hysteresis loss per volume versus frequency for stress versus strain (square) and flux density versus strain (circles).

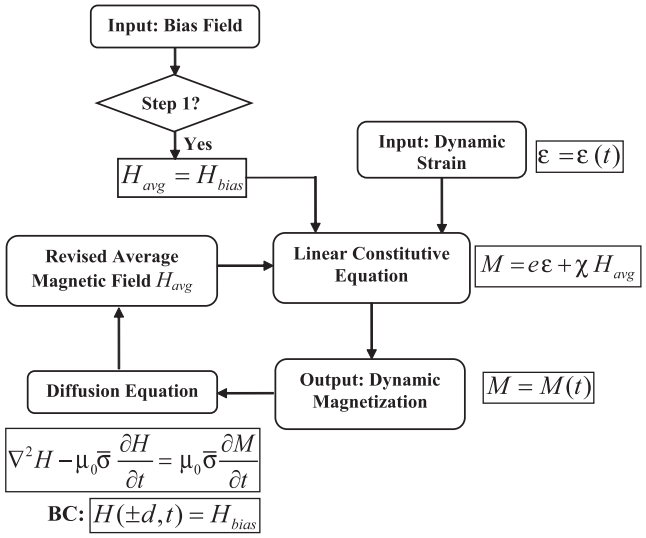


**Figure 4.** Strategy for modeling the frequency dependences in magnetization versus strain hysteresis.

The demagnetization factor $N_d$ depends on the geometry of the sample. For the sample utilized in this study ($6 \times 6 \times 10$ mm$^3$), it is evaluated as 0.385. Although the susceptibility of the material varies with both field and strain, for the sake of simplicity it is assumed to be constant, $\chi = 2.32$.

Figure 3 shows the hysteresis loss for the stress versus strain and flux density versus strain plots. It is observed that the 'mechanical' loss in stress versus strain curves is around 1–2 orders of magnitude higher than the 'magnetomechanical' loss in the flux density versus strain curves. Also, the hysteresis in the stress plots is relatively flat over the measured frequency range, whereas the hysteresis in the flux density increases about 10 times at 160 Hz compared to the quasi-static case. The volumetric energy loss, i.e. the area of the hysteresis loop, is approximately linearly proportional to the frequency. The bias field of 368 kA m$^{-1}$ is strong enough to ensure that the 180° domains disappear within each twin variant, hence each variant consists of a single magnetic domain throughout the cyclic loading process [18]. Therefore, the only parameter affecting the magnetization hysteresis is the rotation angle of the magnetization vectors with respect to the easy $c$ axis. This angle is independent of the strain and variant volume fraction [18] and is therefore a constant for a given bias field.

## 3. Model for frequency-dependent magnetization versus strain hysteresis

A continuum thermodynamics constitutive model has been developed to describe the quasi-static stress and flux density dependence on strain at varied bias fields [18]. The hysteretic stress versus strain curve is dictated by the evolution of the variant volume fractions. We propose that the evolution of volume fraction is independent of frequency for the given range, and therefore no further modification is required to model the stress versus strain behavior at higher frequencies. However, the magnetization dependence on strain changes significantly with increasing frequency due to the losses associated with the dynamic magnetization rotation resulting from mechanical loading. The modeling strategy is summarized in figure 4.

The constitutive model [17] shows that, at high bias fields, the dependence of flux density on strain is almost linear and non-hysteretic. Therefore, a linear constitutive equation for magnetization is assumed as an adequate approximation at quasi-static frequencies. This expression is modified to address dynamic effects. If the strain is applied at a sufficiently slow rate, the magnetization response can be approximated as follows:

$$M = e\varepsilon + \chi H_{\text{avg}} \tag{8}$$

where $e$ and $\chi$ are constants dependent on the given bias field. For the given data, these constants are estimated as $e = -4.58 \times 10^6$ A m$^{-1}$, and $\chi = 2.32$. The average field $H_{\text{avg}}$ acting on the material is not necessarily equal to the bias field $H_{\text{bias}}$.

Equation (8) works well at low frequencies. However, as the frequency increases, consideration of dynamic effects becomes necessary. The dynamic losses are modeled using a 1D diffusion equation that describes the interaction between the dynamic magnetization and the magnetic field inside the material:

$$\nabla^2 H - \mu_0 \bar{\sigma} \frac{\partial H}{\partial t} = \mu_0 \bar{\sigma} \frac{\partial M}{\partial t}, \tag{9}$$

where $\bar{\sigma}$ is the conductivity of the material. This treatment is similar to that in [20] for dynamic actuation, although the final form of the diffusion equation and the boundary conditions are different. The boundary condition on the two faces of the sample is the applied bias field,

$$H(\pm d, t) = H_{\text{bias}}. \tag{10}$$

Although the field on the edges of the sample is constant, the field inside the material varies as dictated by the diffusion equation. The diffusion equation is numerically solved using the backward difference method to obtain the magnetic field at a given position and time $H(\bar{x}, t)$ inside the material.

For sinusoidal applied strain, the magnetization given by equation (8) varies in a sinusoidal fashion. This magnetization change dictates the variation of the magnetic field inside the material given by (9). The internal magnetic field thus varies in a sinusoidal fashion as seen in figure 5(a). The magnitude of variation increases with increasing depth inside the material. In order to capture the bulk material behavior, the average of the internal field is calculated by

$$H_{\text{avg}}(t) = \frac{1}{N_x} \sum_{\bar{X}=-\bar{X}_d}^{\bar{X}_d} H(\bar{x}, t), \tag{11}$$

where $N_x$ represents the number of uniformly spaced points inside the material where the field waveforms are calculated.

Figure 5 shows the results of various stages in the model. We have conducted model simulations for five frequency values, from 4 to 140 Hz, to illustrate the ability of the model to describe the increasing hysteresis with frequency. The parameters used for the presented case are $\mu_r = 3.0$, $\rho = 1/\bar{\sigma} = 62 \times 10^{-8}$ Ω m, and $N_x = 40$. Figure 5(a) shows the magnetic field at various depths inside the sample for a loading frequency of 140 Hz. It is seen that, as the depth inside the sample increases, the variation of the magnetic field increases. At the edges of the sample ($x = \pm d$), the magnetic field is constant, with a value equal to the applied bias field.

Figure 5(b) shows the variation of the average field at varied frequencies. The variation of the average field is directly proportional to the frequency of applied loading: as the frequency increases, the amplitude of the average field increases. Finally, the magnetization is recalculated by using the updated value of the average field as shown by the block diagram in figure 4. The flux density is obtained from the magnetization (see figure 5(c)) by accounting for the demagnetization factor. It is seen that the model adequately captures the increasing hysteresis in flux density with increasing frequency. Further refinements in the model are possible, such as including a 2D diffusion equation, and updating the permeability of the material while numerically solving the diffusion equation.

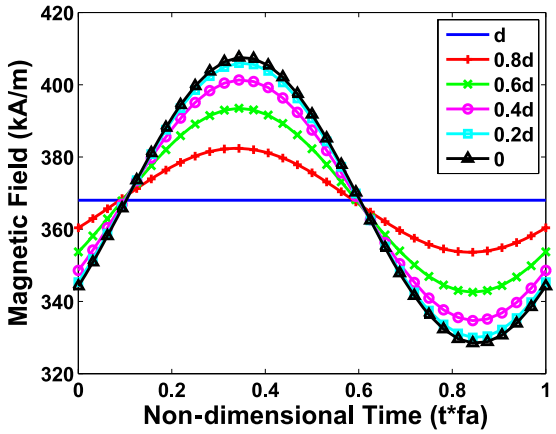


(a)

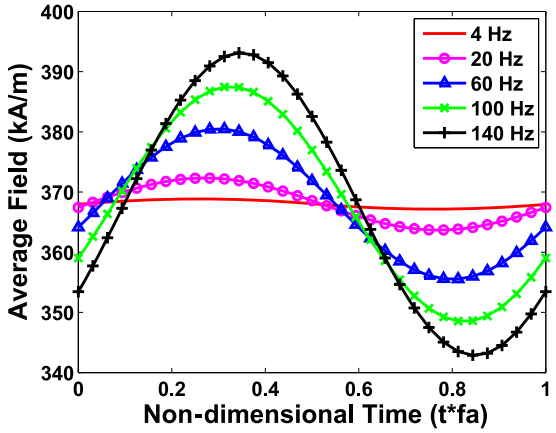


(b)

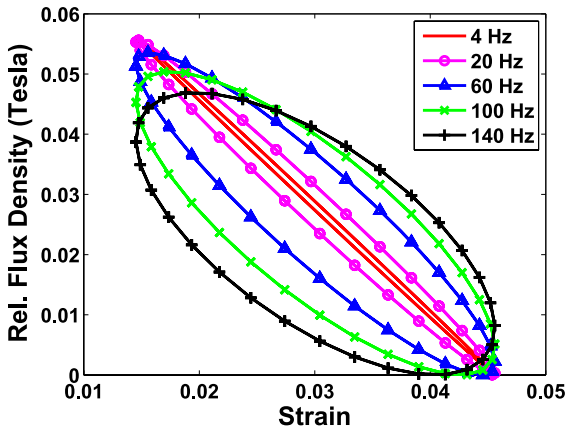


(c)

**Figure 5.** Model results: (a) internal magnetic field versus time at varying depth for the case of 140 Hz strain loading (sample dimension: $\pm d$), (b) average magnetic field versus time at varying frequencies and (c) flux density versus strain at varying frequencies.

## 4. Discussion

The magnetization and stress response of single-crystal Ni–Mn–Ga subjected to dynamic strain loading for frequencies from 0.2 to 160 Hz are presented. This frequency range is significantly higher than in previous sensing characterizations of Ni–Mn–Ga which investigated frequencies from d.c. to only 10 Hz. The rate of twin-variant reorientation remains unaffected by frequency; however, the rate of rotation of magnetization vectors away from the easy $c$ axis is lower than the rate of loading and of twin-variant reorientation. This behavior can be qualitatively explained by the dynamics of a first-order system associated with the rotation of magnetization vectors. The increasing hysteresis in the flux density could complicate the use of this material for dynamic sensing. However, the 'sensitivity' of the material, i.e. net change in flux density per percentage strain input, remains relatively unchanged (≈190 G per % strain) with increasing frequency. Thus the material retains the advantage of being a large deformation, high-compliance sensor as compared to materials such as Terfenol-D [17] at relatively high frequencies. The significant magnetization change at structural frequencies also illustrates the feasibility of using Ni–Mn–Ga for energy harvesting applications. To employ

the material as a dynamic sensor or in energy harvesting applications, permanent magnets can be used instead of an electromagnet. The electromagnet provides the flexibility of turning the field on and off at a desired magnitude, but the permanent magnets provide an energy efficiency advantage. The dynamic magnetization process in the material is modeled using a linear constitutive equation, along with a 1D diffusion equation similar to that used in a previous dynamic actuation model. The model adequately captures the frequency-dependent magnetization versus strain hysteresis and describes the dynamic sensing behavior of Ni–Mn–Ga. As the applied strain frequency increases, magnetic diffusion becomes a more important contributor to magnetization dynamics. As this happens, the effective magnetic field in the material starts to significantly deviate from the bias value. These large fluctuations manifest as increased hysteresis in the flux density versus strain curves. There has been no prior modeling or experimental characterization work on dynamic sensing in Ni–Mn–Ga. The presented model provides an accurate framework which utilizes magnetic diffusion and conventional coupled constitutive modeling to describe the dynamic sensing behavior of Ni–Mn–Ga.

## Acknowledgments

This work was supported in part by the National Science Foundation under grant CMS-0409512, Dr Shih-Chi Liu, program director. We are grateful to the member organizations of the Smart Vehicle Concepts Center (www.SmartVehicleCenter.org) and the National Science Foundation Industry/University Cooperative Research Centers program (www.nsf.gov/eng/iip/iucrc) for providing financial support. Additional support for NS was provided by the Smart Vehicle Concepts Center Fellowship Program.

## References

[1] Soderberg O, Ge Y, Sozniov A, Hannula S and Lindroos V K 2005 Recent breakthrough development of the magnetic shape memory effect in Ni–Mn–Ga alloys *Smart Mater. Struct.* **14** S223–35

[2] Kiang J and Tong L 2005 Modelling of magneto-mechanical behaviour of Ni–Mn–Ga single crystals *J. Magn. Magn. Mater.* **292** 394–412

[3] Henry C P 2002 Dynamic actuation response of Ni–Mn–Ga ferromagnetic shape memory alloys *PhD Thesis* Massachusetts Institute of Technology

[4] Peterson B 2006 Acoustic assisted actuation of Ni–Mn–Ga ferromagnetic shape memory alloys *PhD Thesis* Massachusetts Institute of Technology

[5] Marioni M A, O'Handley R C and Allen S M 2003 Pulsed magnetic field-induced actuation of Ni–Mn–Ga single crystals *Appl. Phys. Lett.* **83** 3966–8

[6] Weetman P and Akhras G 2009 Modeling the dynamical response of ferromagnetic shape memory alloy actuators using a dissipative Euler–Lagrange equation *J. Appl. Phys.* **105** 023917

[7] Gauthier J, Hubert A, Abadie J, Chaillet N and Lexcellent C 2007 Original hybrid control for robotic structures using magnetic shape memory alloys actuators *Intelligent Robots and Systems (San Diego, CA, Oct. 2007)* pp 747–52

[8] Gauthier J, Hubert A, Abadie J, Chaillet N and Lexcellent C 2007 Nonlinear Hamiltonian modelling of magnetic shape memory alloy based actuators *Sensors Actuators* A **141** 536–7

[9] Faidley L E, Dapino M J, Washington G N and Lograsso T A 2006 Modulus increase with magnetic field in ferromagnetic shape memory Ni–Mn–Ga *J. Intell. Mater. Syst. Struct.* **17** 123–31

[10] Sarawate N and Dapino M J 2007 Electrical stiffness tuning in ferromagnetic shape memory Ni–Mn–Ga *Smart Structures and Materials (San Diego, CA, March)*; *Proc. SPIE* **6529** 652916

[11] Mullner P, Chernenko V A and Kostorz G 2003 Stress-induced twin rearrangement resulting in change of magnetization in a Ni–Mn–Ga ferromagnetic martensite *Scr. Mater.* **49** 129–33

[12] Straka L and Heczko O 2003 Superelastic response of Ni–Mn–Ga martensite in magnetic fields and a simple model *IEEE Trans. Magn.* **39** 3402–4

[13] Suorsa I, Pagounis E and Ullakko K 2004 Magnetization dependence on strain in the Ni–Mn–Ga magnetic shape memory material *Appl. Phys. Lett.* **84** 4658–60

[14] Suorsa I, Pagounis E and Ullakko K 2004 Voltage generation induced by mechanical straining in magnetic shape memory materials *J. Appl. Phys.* **95** 8054–8

[15] Suorsa I, Pagounis E and Ullakko K 2005 Position dependent inductance based on magnetic shape memory materials *Sensors Actuators* A **121** 136–41

[16] Heczko O 2005 Magnetic shape memory effect and magnetization reversal *J. Magn. Magn. Mater.* **290/291** 787–94

[17] Sarawate N and Dapino M J 2006 Experimental characterization of the sensor effect in ferromagnetic shape memory Ni–Mn–Ga *Appl. Phys. Lett.* **88** 121923

[18] Sarawate N and Dapino M J 2007 A continuum thermodynamics model for the sensing effect in ferromagnetic shape memory Ni–Mn–Ga *J. Appl. Phys.* **101** 123522

[19] Karaman I, Basaran B, Karaca H E, Karsilayan A I and Chumlyakov Y I 2007 Energy harvesting using martensite variant reorientation mechanism in a Ni–Mn–Ga magnetic shape memory alloy *Appl. Phys. Lett.* **90** 172505

[20] Sarawate N and Dapino M J 2008 Frequency dependent strain-field hysteresis model for ferromagnetic shape memory Ni–Mn–Ga *IEEE Trans. Magn.* **44** 566–75

[21] Li G, Liu Y and Ngoi B K A 2005 Some aspects of strain-induced change of magnetization in a Ni–Mn–Ga single crystal *Scr. Mater.* **53** 829–34

[22] Uchino K and Hirose S 2001 Loss mechanisms in piezoelectrics: how to measure different losses separately *IEEE Trans. Ultrason. Ferroelectr. Freq. Control* **48** 307–21

[23] Ercuta A and Mihalca I 2002 Magnetomechanical damping and magnetoelastic hysteresis in permalloy *J. Phys. D: Appl. Phys.* **35** 2902–8

[24] Sarawate N N 2008 Characterization and modeling of the ferromagnetic shape memory alloy Ni–Mn–Ga for sensing and actuation *PhD Thesis* The Ohio State University